ARTICLES

Journal of Semiconductors
(2019) 40, 032702
doi: 10.1088/1674-4926/40/3/032702

Optimization of broadband omnidirectional antireflection coatings for solar cells

Xia Guo[1, †], Qiaoli Liu[1, 2], Huijun Tian[1, 3], Ben Li[2], Hongyi Zhou[2], Chong Li[2], Anqi Hu[1], and Xiaoying He[1, †]

[1]School of Electronic Engineering, State Key Laboratory for Information Photonics and Optical Communications, Beijing Key Laboratory of Work Safety Intelligent Monitoring, Beijing University of Posts and Telecommunications, Beijing 100876, China

[2]School of Information, Beijing University of Technology, Beijing 100124, China

[3]Institute of Laser Engineering, Beijing University of Technology, Beijing 100124, China

Abstract: Broadband and omnidirectional antireflection coating is generally an effective way to improve solar cell efficiency, because the destructive interference between the reflected and incident light can maximize the light transmission into the absorption layer. In this paper, we report the incident quantum efficiency η_{in}, not incident energy or power, as the evaluation function by the ant colony algorithm optimization method, which is a swarm-based optimization method. Also, SPCTRL2 is proposed to be incorporated for accurate optimization because the solar irradiance on a receiver plane is dependent on position, season, and time. Cities of Quito, Beijing and Moscow are selected for two- and three-layer antireflective coating optimization over λ = [300, 1100] nm and θ = [0°, 90°]. The η_{in} increases by 0.26%, 1.37% and 4.24% for the above 3 cities, respectively, compared with that calculated by other rigorous optimization algorithms methods, which is further verified by the effect of position and time dependent solar spectrum on the antireflective coating design.

Key words: antireflection coating; ant colony algorithm; incident quantum efficiency; SPCTRL2

Citation: X Guo, Q L Liu, H J Tian, B Li, H Y Zhou, C Li, A Q Hu, and X Y He, Optimization of broadband omnidirectional antireflection coatings for solar cells[J]. *J. Semicond.*, 2019, 40(3), 032702. http://doi.org/10.1088/1674-4926/40/3/032702

1. Introduction

Broadband and omnidirectional antireflection is one of the most desirable characteristics for high-efficiency solar cells to allow maximum light transmission into the absorption layer[1, 2]. Antireflection (AR) can be achieved by a few additional layers outside of Si solar cells that occupy about 80% of the photovoltaic market due to the mature technology and low price[3, 4]. As early as 1880 it was found that multilayer films with graded refractive-index increasing from top to bottom between air and the Si substrate have broadband transmittance both at normal and oblique incident angles[5–8]. Insect compound eyes are one of the typical graded refractive-index structures which have inspired the development of lots of nanostructure and fabrication techniques in recent years, such as SiO_2 microsphere arrays[9, 10], Si nanowires[11, 12], nanorods[13–15], Si nanostructure arrays[16], etc. The minimum refractive index reached 1.05 using oblique-angle deposition techniques, which are highly desirable for antireflective coatings[17–19]. In the view of the effective medium theory (EMT), light is bent progressively in the ARs with smoothly graded refractive index changing profile from air to substrate[20, 21]. Generally, different refractive index profile curves, such as linear, parabolic, cubic, quantic, exponential and exponential-sinusoidal, exhibit different antireflective performance. The optimization of the refractive-index profile experimentally is then changed to optimize the profile of the nanostructure and its filling factor[22, 23]. However, it is still a great challenge to obtain a high-performance optical structure compared with the optical performance characterization of a structure[24–26]. Recently, several rigorous optimization algorithms based on advanced global optimization techniques, such as the genetic algorithm[27, 28], simulated annealing algorithm[29, 30] and artificial immune algorithm[31] have been developed to optimize multilayer AR coating design. Recently, various swarm-based optimization algorithms have been successfully implemented in the design of multilayer AR coating to improve the existing numerical methods. These optimization methods are robust, stochastic and generally do not rely on the initial conditions. Among them, ant colony algorithm (ACA)[32] is a heuristic optimization algorithm that mimicks the way ants establish the shortest path from their nest to the food source and back by leaving their pheromones on the path as a communication medium among them[32]. A moving ant releases quantities of pheromone on the way, and the other ants detect and evaluate the choice of route according to the pheromone trail. Finally, the shortest path can be found after more and more ants select a more intense pheromone way. It has proved to be a powerful method to solve the optimization problems in basic and applied science[33]. It also demonstrated the best optimization result in the AR coating system. An average reflectance of 2.98% was obtained, which is much lower than 4.5% optimized by the genetic algorithm and 6.59% by the simulated annealing algorithm over the optimization range of λ = [400, 1100] nm and θ = [0°, 80°][34].

There are two problems with the current optimization algorithms. The first problem is that it is the reflectance or transmittance, which is the concept of energy, that is utilized in the

Correspondence to: X Guo, guox@bupt.edu.cn; X Y He, xiaoyinghe@bupt.edu.cn

Received 5 SEPTEMBER 2018; Revised 6 OCTOBER 2018.

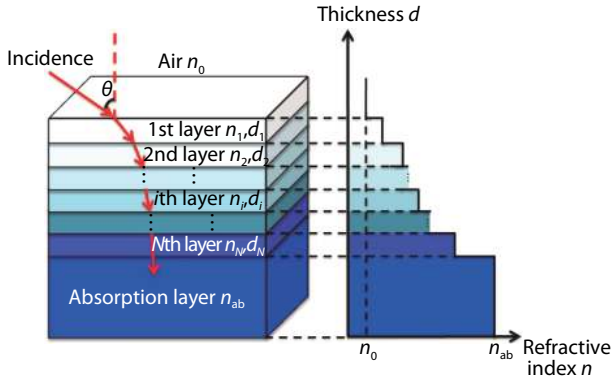

Fig. 1. (Color online) The graded refractive-index structure of an N-layer anti-reflective coating system. A plane wave is incident from the air with the refractive index of n_0 and incident angle of θ. Every layer of the coating is characterized by the thickness d_i with the refractive index n_i, $i = \{1, 2, \ldots, N\}$. The entire absorption layer is assumed to be in the bottom layer with refractive index n_{ab} without the back surface reflectance. The right curve shows the numerical value of the graded change of refractive index and the thickness of each anti-reflective layer.

evaluation function for all the above algorithms. However, it should be the incident quantum efficiency η_{in} which is the concept of particle that should be the objective. Another problem is the actual solar spectrum is position and time dependent. While in the above optimization, uniform irradiation is applied for simplicity. The existing inaccurate selections of the evaluation function and solar spectrum indicate there is space to further improve the quantum efficiency of the solar cells.

In this paper, the incident quantum efficiency η_{in} is proposed to be the evaluation function for the optimization of broadband omnidirectional antireflective coating using the ACA method. SPCTRL2[35], a program computing solar irradiance of clear sky spectral direct beams on a receiver plane at a position and time, is also incorporated in the optimization. Three typical cities of Quito, Beijing and Moscow, which are located at the equator and northern latitudes of 39.9° and 55.3°, respectively, are selected for AR optimization over θ = [0°, 90°] and λ = [300, 1100] nm. The incident quantum efficiency of two-layer AR coating optimized by ACA with SPCTRL2 incorporated increases from 95.74% to 96.00% for Quito, from 92.27% to 93.64% for Beijing, and from 86.78% to 91.02% for Moscow, respectively. With three-layer AR, the η_{in} increases from 96.86% to 97.60% for Quito, from 95.72% to 97.03% for Beijing, and from 94.46% to 95.74% for Moscow. These comparable results suggest that using η_{in} as the evaluation function in ACA method incorporated with actual solar spectra can practically improve the quantum efficiency of solar cells.

2. Simulation approach

2.1. Modelling structure and evaluation function

The schematic structure of the graded refractive-index antireflective coating to be optimized is shown in Fig. 1, where a plane wave is incident from the air with an incident angle of θ and refractive index of n_0. Each layer is characterized by its thickness d_i with the refractive index n_i, $i = \{1, 2, \ldots, N\}$. For simplicity, the entire absorption layer is assumed to be at the bottom absorption layer with refractive index of n_{ab} without considering the back surface reflectance. For practical materials, the refractive index and the extinction coefficient vary with wavelength, which is known as the dispersion relationship. The refractive index, dispersion and absorption curves can be included into the transmission calculation realized by expanding each refractive index in the optimization into a matrix in the software "MATLAB". The calculations presented here, however, only consider single values of refractive index (i.e. no wavelength dependence) and the layers are assumed to be non-absorbing. The refractive index and AR layer thickness are set as optimization parameters in the ant colony for optimizing AR layer.

The incident quantum efficiency η_{in}, as the evaluation function, which is dependent on the wavelength and incident angle, can be expressed by

$$\eta_{in} = \frac{\int_{\lambda_1}^{\lambda_2}\int_{\theta_1}^{\theta_2} T(\lambda,\theta)\,\mathrm{Num}(\lambda,\theta)\,\mathrm{d}\theta\mathrm{d}\lambda}{\int_{\lambda_1}^{\lambda_2}\int_{\theta_1}^{\theta_2} \mathrm{Num}(\lambda,\theta)\,\mathrm{d}\theta\mathrm{d}\lambda}, \quad (1)$$

in which λ_2 and λ_1 are the upper and lower boundaries of the wavelength, respectively. θ_2 and θ_1 are the upper and lower boundaries of the incident angle, respectively. $T(\lambda, \theta)$ is the optical transmittance of the N-layer antireflective coating and is calculated by the transmission matrix method according to the Maxwell equations. The Num(λ, θ) (photon/m^2/s) is a function of the incident wavelength λ and the incident angle θ, which can be expressed by[36, 37]

$$\mathrm{Num}(\lambda,\theta) = E(\lambda,\theta)\frac{\lambda}{hc}, \quad (2)$$

where h is Planck's constant and c is the speed of light in vacuum. $E(\lambda, \theta)$ (in units of W/m^2/micron interval) is the irradiance of the solar spectrum. SPCTRL2, a program from the National Renewable Energy Laboratory, can provide detailed solar spectrum data in the world which considers the longitude, latitude, atmospheric conditions, and incident angle with a date and a time. All the data of the irradiance of the solar spectrum $E(\lambda, \theta)$ and the incident photon flux density Num(λ, θ) are obtained from SPCTRL2 in this report. With the revolution of the earth, the incident angle in the south-north direction varies seasonally with the oscillation centre on the day of spring or autumn equinox, when the sunlight is normally incident on the equator. Hence, the AR optimization which should consider the local solar spectrum of a whole year is now simplified to consider the solar spectrum on the day of spring equinox only.

2.2. Solar spectrum

Fig. 2 shows the spectra of the daytime incident photon flux density on the day of the spring equinox for the cities of (a) Quito, (b) Beijing and (c) Moscow according to Eq. (2). The input parameters in the SPCTRL2 for the cities of Quito, Beijing and Moscow are shown in Table 1, which are all from AERONET[37]. For Quito, the incident angle changes from 90° to 0° then back to 90° which corresponds to the period from sunrise, to noon, then to sunset, because the two-dimensional incident plane is the same from sunrise to sunset. The minimum incident angle is 0°, which is shown in Fig. 2(a). However, for the cities in the southern or northern hemisphere, the two-dimensional incident plane changes all the time from sunrise to sunset. The minimal incident angle is determined by the relative position of the Sun and the Earth. The incident angle

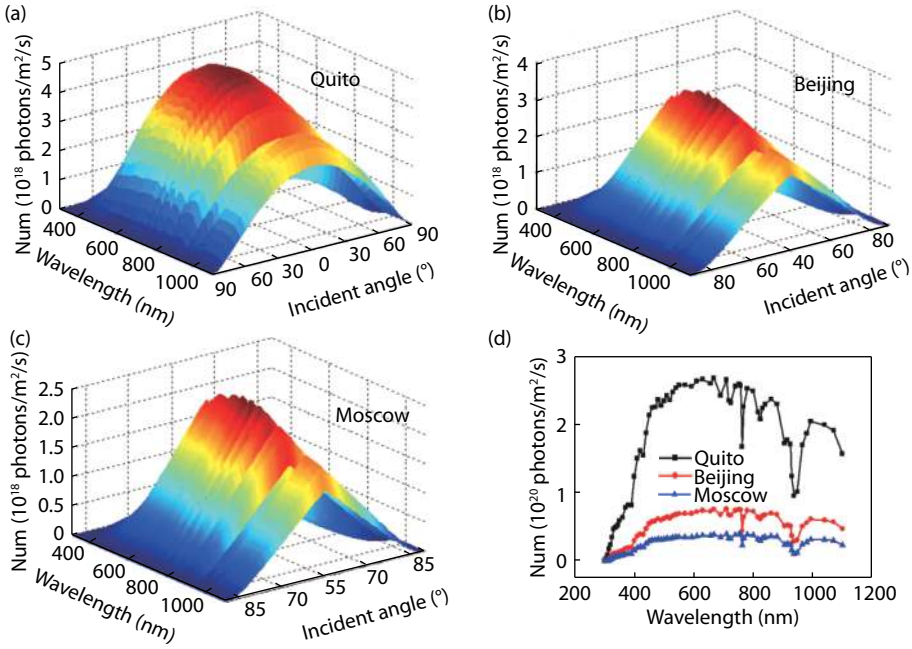

Fig. 2. (Color online) The dependence of the incident photon flux density on the wavelength and the incident angle on the day of the spring equinox for (a) Quito, (b) Beijing and (c) Moscow, respectively. At noon of the day of the spring equinox, the sunlight is vertically incident on the equator. The incident angle at noon of the day of spring equinox for Quito, Beijing and Moscow is 0, 40, and 55 degrees, respectively. At sunrise or sunset, the incident angles of these three cities are the same 90 degrees. (d) The comparison of the spectrum of the incident photon flux density of three cities at noon on the day of the spring equinox. The incident photon flux density spectra are totally different Earth due to the atmosphere scatter and absorption at different location with different incident angle and latitude.

Table 1. Input parameters used in SPCTRL2 program.

Parameter	Latitude (°)	Longitude (°)	Aerosol optical depth	Alpha	Albedo (surface reflectance)	Total column ozone (cm)	Total precipitable water vapor (cm)	Surface pressure (mB)	Days of the year
Quito	0	78.5W	0.27	1.14	0.2	0.34	1.42	1013.25	79
Beijing	39.9N	116.3E	0.77	1.14	0.16	0.34	0.95	1040	79
Moscow	55.3N	37.5E	0.35	1.14	0.1	0.36	1.36	750	79

Table 2. Detail structures of two-layer antireflective coating optimized by ant colony algorithm with and without SPCTRL2 incorporated.

Optimization method	1st layer		2nd layer	
	Refractive index	Thickness (nm)	Refractive index	Thickness (nm)
No SPCTRL2	1.41	112.09	2.41	58.89
SPCTRL2 at Quito	1.44	113.66	2.55	60.46
SPCTRL2 at Beijing	1.27	165.29	2.29	76.10
SPCTRL2 at Moscow	1.17	221.62	2.15	80.80

changes from 90° to 39.9° and then to 90° for Beijing from sunrise to sunset, as shown in Fig. 2(b). For the same reason, the minimum incident angle is 55.3° for Moscow, as shown in Fig. 2(c). Therefore, the boundaries of the incident angle in Eq. (1) will change with the actual location of the solar cells. Fig. 2(d) compares the incident photon flux density spectra the solar cell will receive over the day of the spring equinox when placed in Quito, Beijing and Moscow, after integrating over the entire incident angle range. The incident photon flux density spectra are totally different on Earth due to the atmosphere scatter and absorption at different locations with different incident angle and latitude.

3. Results and discussion

Table 2 presents the detailed structures of two AR coating films optimized by the ACA method with and without SPCTRL2 incorporated. Fig. 3(a) shows the optimized optical transmittance spectrum optimized by ACA without considering SPCTRL2 with λ = [300, 1100] nm and θ = [0°, 90°], where the area of the contour plot with the transmittance above 80% and 98% are 76.12% and 27.51%, respectively, which are marked by white lines. Figs. 3(b)–3(d) presents the optimized optical transmittance spectrum, wherein $\eta_{\text{in-Q}}$, $\eta_{\text{in-B}}$ and $\eta_{\text{in-M}}$ represent the η_{in} of Quito, Beijing and Moscow, respectively. The η_{in} are 95.74%, 92.27%, and 86.78% for Quito, Beijing and Moscow, respectively. Obviously, the area with higher transmittance redshifts and moves up to larger incident angle in order to adapt to the effect of the city location and time in the optimization, which can be distinguished from the contour lines of the transmittance. The area of the contour plot with the trans-

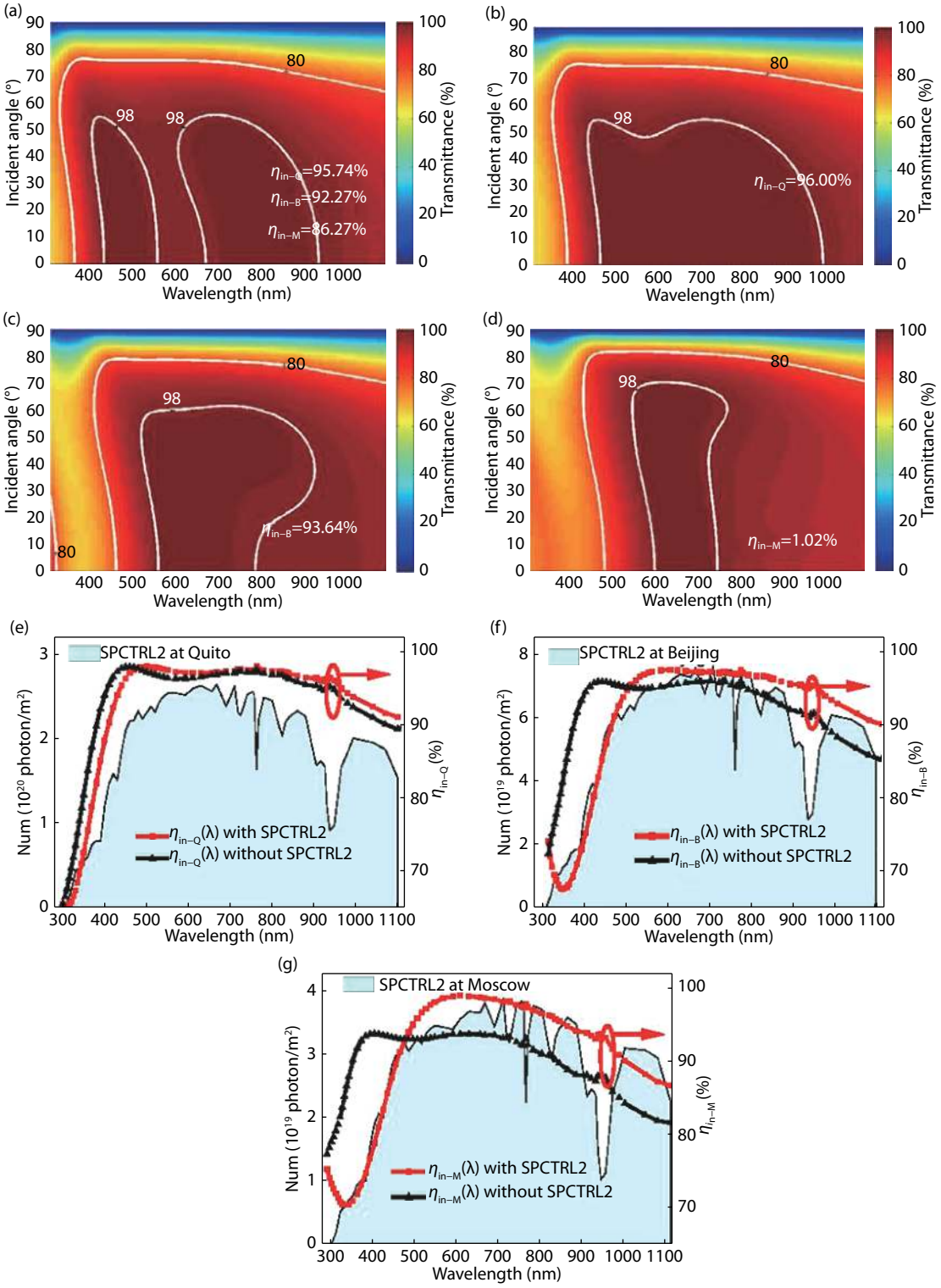

Fig. 3. (Color online) The optical transmittance spectrum with λ = [300, 1100] nm and θ = [0°, 90°] for two-layer AR coating optimized by (a) ACA without SPCTRL2, and with SPCTRL2 of (b) Quito (c) Beijing and (d) Moscow. The detail structures are presented in Table 2. The areas with transmittance above 80% and 98% are marked by white lines. The incident quantum efficiency at Quito, Beijing and Moscow optimized by ACA with SPCTRL2 incorporated is 0.26%, 1.37% and 4.24% larger than that optimized without SPCTRL2 incorporated for two-layer AR coating, respectively. Comparison of the actual solar spectrum and incident quantum efficiency η_{in} (λ), for (e) Quito (f) Beijing and (g) Moscow with and without SPCTRL2 incorporated. When considering the solar spectrum in different cities and setting η_{in} as the evaluation function in the AR coating optimization, the peak of the quantum efficiency spectrum moves towards around 700 nm, which is the peak of the actual solar spectrum and fits the actual solar spectrum very well for all three cities.

mittance above 80% and 98% are 73.72% and 35.99%, 71.32% and 27.12%, 69.92% and 17.43%, respectively. However, the η_{in} for Quito, Beijing and Moscow are increased to 96.00%, 93.64%, and 91.02%, respectively. In other words, the incident quantum efficiency at Quito, Beijing and Moscow optimized by the ant colony algorithm with SPCTRL2 incorporated are

0.26%, 1.37% and 4.24% larger than that optimized without SPCTRL2 incorporated for two-layer antireflective coating, respectively. Figs. 3(e)–3(g) show the omnidirectional incident quantum efficiencies $\eta_{in}(\lambda)$ of Quito, Beijing and Moscow with and without SPCTRL2 incorporated, respectively. It can be seen that, with SPCTRL2 incorporated, the quantum efficiency spectrum almost fits the actual solar spectrum very well for each city. While for the quantum efficiency spectrum optimized without SPCTRL2 incorporated, there is an obvious mismatch between the actual solar spectrum and quantum efficiency spectrum. Similar results are also obtained for three-layer AR coating optimization. The η_{in} increases from 96.86% to 97.60% for Quito, from 95.72% to 97.03% for Beijing, and from 94.46% to 95.74% for Moscow, respectively.

In practice, the refractive index value of bulk material between 1.46 and 2.55 is available for common silicon solar cells, which limits the current commercial availability of low-refractive index materials in solar cell applications. Two-layer and three-layer AR coatings are optimized with the restriction of refractive index between 1.46 and 2.55. Compared with the refractive index ranging from 1.05 to 2.66, the η_{in} of two-layer AR coating optimized with and without SPCTRL2 incorporated at Quito, Beijing and Moscow are 96.00% and 95.30%, 93.64% and 92.83%, 91.02% and 87.71%, respectively. For three-layer AR coating, it is 97.60% and 95.96%, 97.03% and 93.02%, 95.74% and 87.94%, respectively. The improvement is still obvious. It is necessary to perform careful optimization for AR coatings in practice even with restrictions on the refractive index selection, especially for the cities in the high latitude. Comparing the detailed structure parameters, it was found that the lower limit of the refractive index is more important for η_{in}, because the large discrepancy of the refractive index between the air and surface layer of the solar cells determines the reflection. Expanding the range of the refractive index for the practical material can be achieved by nano-technology and advanced deposition techniques, which has proven to be a useful technique to manipulate the light coupling in silicon photonics.

4. Conclusion

In this paper, the incident quantum efficiency η_{in} is set as the evaluation function with SPCTRL2 program incorporated to optimize the broadband and omnidirectional AR coating by the ACA method for silicon solar cells for the purpose of practical applications. The solar spectrum on the day of the spring equinox was selected, which can simplify the optimization process to expand to whole year optimization. Two-layer and three-layer antireflective coatings are optimized over λ = [300, 1100] nm and θ = [0°, 90°]. The η_{in} of two-layer AR coating optimized by the ACA method with SPCTRL2 incorporated increases by 0.26%, 1.37% and 4.24% over that without SPCTRL2 incorporated for Quito, Beijing and Moscow, respectively. While for three-layer antireflective coating, the η_{in} are improved by 0.74%, 1.31% and 1.28%, respectively. The careful optimization for AR coatings in practice even with restrictions on the refractive index selection can further improve the efficiency of the solar cells, especially for high latitude locations.

Acknowledgements

This work was supported by the National Key Research and Development of China (No. 2017YFF0104801) , the National Natural Science Foundation of China (Nos. 61675046, 61804012), and the Open Fund of IPOC (No. IPOC2017B011).

References

[1] Leem J W, Guan X Y, Choi M, et al. Broadband and omnidirectional highly-transparent coverglasses coated with biomimetic moth-eye nanopatterned polymer films for solar photovoltaic system applications. Sol Energy Mater Sol C, 2015, 134, 45

[2] Rahman A, Ashraf A, Xin H, et al. Sub-50-nm self-assembled nanotextures for enhanced broadband antireflection in silicon solar cells. Nat Commun, 2015, 6, 5963

[3] Tyagi V V, Rahim N A A, Rahim N A, et al. Progress in solar, PV technology: research and achievement. Renew Sust Energy Rev, 2013, 20, 443

[4] Louwen A, Sark W V, Schropp R, et al. A cost roadmap for silicon heterojunction solar cells. Sol Energ Mat Sol C, 2016, 147, 295

[5] Rayleigh L. On reflection of vibrations at the confines of two media between which the transition is gradual. Proc London Math Soc, 1879, 1(1), 51

[6] Carlson D E, Wronski C R. Amorphous silicon solar cell. Appl Phys Lett, 1976, 28(11), 671

[7] Zeng L, Yi Y, Hong C, et al. Efficiency enhancement in Si solar cells by textured photonic crystal back reflector. Appl Phys Lett, 2006, 89(11), 111111

[8] Xiong C, Xu W, Zhao Y, et al. New design graded refractive index antireflection coatings for silicon solar cells. Mod Phys Lett B, 2017, 31(19–21), 1740028

[9] Tao M, Zhou W, Yang H, et al. Surface texturing by solution deposition for omnidirectional antireflection. Appl Phys Lett, 2007, 91(8), 081118

[10] Bett A, Eisenlohr J, Höhn O, et al. Front side antireflection concepts for silicon solar cells with diffractive rear side structures. 29th European Photovoltaic Solar Energy Conference and Exhibition, 2014: 987.

[11] Yang J, Luo F, Kao T S, et al. Design and fabrication of broadband ultralow reflectivity black Si surfaces by laser micro/nanoprocessing. Light Sci Appl, 2014, 3(7), e185

[12] Huang Y F, Chattopadhyay S, Jen Y J, et al. Improved broadband and quasi-omnidirectional anti-reflection properties with biomimetic silicon nanostructures. Nat Nanotech, 2007, 2(12), 770

[13] Diedenhofen S L, Vecchi G, Algra R E, et al. Broad-band and omnidirectional antireflection coatings based on semiconductor nanorods. Adv Mater, 2009, 21(9), 973

[14] Wang Z S, Kawauchi H, Kashima T, et al. Significant influence of TiO_2 photoelectrode morphology on the energy conversion efficiency of N719 dye-sensitized solar cell. Coord Chem Rev, 2004, 248(13/14), 1381

[15] Keis K, Magnusson E, Lindström H, et al. A 5% efficient photoelectrochemical solar cell based on nanostructured ZnO electrodes. Sol Energ Mat Sol C, 2002, 73(1), 51

[16] Cai J, Qi L. Recent advances in antireflective surfaces based on nanostructure arrays. Mater Horiz, 2015, 2(1), 37

[17] Xi J Q, Schubert M F, Kim J K, et al. Optical thin-film materials with low refractive index for broadband elimination of Fresnel reflection. Nat Photonics, 2007, 1(3), 176

[18] Guter W, Schöne J, Philipps S P, et al. Current-matched triple-junction solar cell reaching 41.1% conversion efficiency under concentrated sunlight. Appl Phys Lett, 2009, 94(22), 223504

[19] Liang Y, Feng D, Wu Y, et al. Highly efficient solar cell polymers developed via fine-tuning of structural and electronic properties. J Am Chem Soc, 2009, 131(22), 7792

[20] Hiramoto M, Fujiwara H, Yokoyama M. Three-layered organic solar cell with a photoactive interlayer of codeposited pigments. Appl Phys Lett, 1991, 58(10), 1062

[21] Spinelli P, Verschuuren M, Polman A. Broadband omnidirectional antireflection coating based on subwavelength surface Mie resonators. Nat Commun, 2012, 3, 692

[22] Campbell W M, Burrell A K, Officer D L, et al. Porphyrins as light harvesters in the dye-sensitised TiO_2 solar cell. Coord Chem Rev, 2004, 248(13/14), 1363

[23] Krebs F C, Tromholt T, Jørgensen M. Upscaling of polymer solar cell fabrication using full roll-to-roll processing. Nanoscale, 2010, 2(6), 873

[24] Liao H H, Chen L M, Xu Z, et al. Highly efficient inverted polymer solar cell by low temperature annealing of Cs_2CO_3 interlayer. Appl Phys Lett, 2008, 92(17), 156

[25] Barkhouse D A R, Gunawan O, Gokmen T, et al. Device characteristics of a 10.1% hydrazine-processed $Cu_2ZnSn(Se, S)_4$ solar cell. Prog Photovolt: Res Appl, 2012, 20(1), 6

[26] Blakers A W, Wang A, Milne A M, et al. 22.8% efficient silicon solar cell. Appl Phys Lett, 1989, 55(13), 1363

[27] Poxson D J, M F Schubert M F, Mont F W, et al. Broadband omnidirectional antireflection coatings optimized by genetic algorithm. Opt Lett, 2009, 34(6), 728

[28] Oh S J, Chhajed S, Poxson D J, et al. Enhanced broadband and omni-directional performance of polycrystalline Si solar cells by using discrete multilayer antireflection coatings. Opt Express, 2013, 21(101), A157

[29] Chang Y J. Suppressing lossy-film-induced angular mismatches between reflectance and transmittance extrema: optimum optical designs of interlayers and AR coating for maximum transmittance into active layers of CIGS solar cells. Opt Express, 2014, 22(101), A167

[30] Chang Y J, Chen Y T. Broadband omnidirectional antireflection coatings for metal-backed solar cells optimized using simulated annealing algorithm incorporated with solar spectrum. Opt Express, 2011, 19(104), A875

[31] Wang W. Design of nonpolarizing antireflection coating by using multiobjective optimization algorithm. Optik, 2013, 124(16), 2482

[32] Guo X, Zhou H Y, Guo S, et al. Design of broadband omnidirectional antireflection coatings using ant colony algorithm. Opt Express, 2014, 22(104), A1137

[33] Dorigo M, Gambardella L M. Ant colony system: a cooperative learning approach to the traveling salesman problem. IEEE Trans Evolut Comput, 1997, 1(1), 53

[34] Bird R E, Riordan C. Simple solar spectral model for direct and diffuse irradiance on horizontal and tilted planes at the earth's surface for cloudless atmospheres. SPIE, 1993, 54, 171

[35] Asadollahbaik A, Boden S A, Charlton M D, et al. Reflectance properties of silicon moth-eyes in response to variations in angle of incidence, polarisation and azimuth orientation. Opt Express, 2014, 22(102), A402

[36] Boden S A, Bagnall D M. Sunrise to sunset optimization of thin film antireflective coatings for encapsulated, planar silicon solar cells. Prog Photovolt: Res Appl, 2009, 17(4), 241

[37] Holben B N, Eck T F, Slutsker I, et al. AERONET-A federated instrument network and data archive for aerosol characterization. Remote Sens Environ, 1998, 66(1), 1